Proc. of the IEEE Conf. on Computer Vision and Pattern Recognition Maui, HI, June 1991, pp 371-377.

MIT Media Lab Vision and Modeling Group TR # 164

Markov/Gibbs Texture Modeling: Aura Matrices and Temperature Effects*

Rosalind W. Picard† Ibrahim M. Elfadel‡ Alex P. Pentland†

Abstract

We use a new "aura" framework to rewrite the nonlinear energy function of a homogeneous anisotropic Markov/Gibbs random field (MRF) as a linear sum of aura measures. The new formulation relates MRF's to co-occurrence matrices. It also provides a physical interpretation of MRF textures in terms of the mixing and separation of graylevel sets, and in terms of boundary maximization and minimization.

Within this framework, we introduce the use of temperature for texture modeling and show how the parameters of the MRF can be interpreted as temperature annealing rates. In particular, we show evidence for a transition temperature, above which all patterns generated will be visually similar, and below which a pattern evolves down to its ground state. Finally, we describe briefly some new results which characterize the ground state patterns.

1 Introduction

Since the establishment of the equivalence between Gibbs and Markov random fields (MRF's), there has been a flurry of application of MRF's to image processing. In particular, MRF's have been shown to be useful for the representation of natural texture patterns, and have consequently been applied to image classification, segmentation, restoration, and coding.

In these applications the MRF is often assumed to be a prior model for the image and its texture. The resulting posterior distribution is then maximized using an annealing algorithm which depends on temperature. However, in the literature examining MRF's as texture models, no studies have been done on the effect of temperature on the texture. Also, no studies have characterized the textures which are formed by maximizing the MRF probability.

This paper begins by showing a way to linearize the Gibbs energy by using the new tool of aura measures. With this formulation, we show that the anisotropic model parameters behave like the rate constant used in temperature annealing. We argue that it is the interplay of these different rates that makes interesting texture patterns occur. We also give evidence for a *transition temperature* above which a pattern will be visually similar, and below which it evolves down to its $T = 0$ equilibrium state, or "ground state". Finally, we discuss some results on the characterization of these ground states using the aura matrices.

2 Background

2.1 Notation

Let the image be represented by a finite rectangular $M \times N$ lattice $\mathcal{S}$ with a neighborhood structure $\mathbf{N} = \{\mathcal{N}_s, s \in \mathcal{S}\}$, where $\mathcal{N}_s \subseteq \mathcal{S}$ is the set of neighbors of the site $s \in \mathcal{S}$. Every site has a graylevel value $x_s \in \Lambda = \{0, 1, \ldots, n-1\}$. We denote by $\mathbf{x}$ the vector $(x_s, 1 \leq s \leq |\mathcal{S}|)$ of site graylevel values. The set of all graylevels of value g is $\mathcal{S}_g = \{s \in \mathcal{S} | x_s = g\}$, $\forall g \in \Lambda$. In this paper, we will assume that the histogram of the image is uniform, so that $|\mathcal{S}_g| = MN/n$. When nothing is known about the texture pattern being modeled, this assumption gives the maximum entropy prior.

For a homogeneous MRF, the neighborhood structure must be symmetric, i.e., $\forall s, r \in \mathcal{S}$, $s \in \mathcal{N}_r$ if and

*This work was supported by the National Science Foundation and the Defense Advanced Research Projects Agency (DARPA) under Grant No. MIP-88-14612, the National Science Foundation under Grant No. IRI-8719920, the Rome Air Development Center (RADC) of the Air Force System Command and the Defense Advanced Research Projects Agency (DARPA) under contract No. F30602-89-C-0022.

†MIT Media Lab, 20 Ames Street, Cambridge MA 02139, picard@media.mit.edu, pentland@media.mit.edu

‡MIT Research Lab of Electronics, 50 Vassar Street, Cambridge MA 02139, elfadel@sobolev.mit.edu

only if $r \in \mathcal{N}_s$. The MRF is usually described by its order, which defines its neighborhood. In this paper, MRF's of order 1-4 are used; these correspond to the four, eight, twelve, and twenty nearest neighbors respectively. The MRF's used in this paper may also be anisotropic, having different weights associated with each pair of symmetric neighbors.

Notice that the first order neighborhood has two principle directions of anisotropy – different weights can be assigned to its horizontal and its vertical neighbors. In general, we can partition any MRF neighborhood into K subneighborhoods, each with only one weighting parameter. We write

$$\mathcal{N}_s = \bigcup_{k=1}^{K} \mathcal{N}_s^k, \ \forall s \in \mathcal{S},$$

where $\mathcal{N}_s^k \cap \mathcal{N}_s^l = \emptyset$, unless $l = k$. For the first order anisotropic MRF, $\mathcal{N}_s^1$ is the horizontal isotropic subneighborhood and $\mathcal{N}_s^2$ is the vertical one.

Throughout this paper we assume periodic boundary conditions: the top of the image is connected to the bottom, and the left to the right. This assumption is not necessary for any of the results in this paper, but helps to simplify notation.

For the periodic lattice $\mathcal{S}$ with the symmetric neighborhood structure $\mathbf{N}$, we define the Gibbs energy

$$E(\mathbf{x}) = \sum_{s\in\mathcal{S}} V_s(x_s) + \sum_{s\in\mathcal{S}} \sum_{r\in\mathcal{N}_s} V_{sr}(x_s, x_r), \qquad (1)$$

where the V_s's are the single-site potentials and the V_{sr}'s are the two-site potentials. The single-site potentials are also called the external field. To this energy, we can assign a random field whose probability distribution is given by

$$P(\mathbf{x}) = \frac{1}{Z}\exp(-\frac{1}{T}E(\mathbf{x})), \qquad (2)$$

where T is the "temperature" of the field and Z is a positive normalizing constant. The most probable configuration for the image corresponds to the one which minimizes the Gibbs energy.

Different distributions can be obtained by specifying the potentials in (1). The autobinomial model [1], which was studied by Cross and Jain for texture modeling [2], is formed when the MRF has binomial conditional probabilities. Its Gibbs energy is $E(\mathbf{x}) =$

$$-\sum_{s\in\mathcal{S}} \left(\alpha_s x_s + T \ln \begin{pmatrix} n-1 \\ x_s \end{pmatrix} + \sum_{r\in\mathcal{N}_s} \beta_{sr} x_s x_r \right). \quad (3)$$

In the homogeneous case $\alpha_s = \alpha$ (site-independent), and the autobinomial bonding parameters $\beta_{sr} = \beta_r$ (site-independent but possibly dependent on the position of the neighbor). The bonding parameters are *isotropic* when $\beta_r = \beta, \ \forall\ r \in \mathcal{N}$. In this paper, the effects of the external field, α_s, can be ignored.

Another popular choice of energy function [3, 4] gives the homogeneous Potts model, for which

$$E(\mathbf{x}) = \sum_{s\in\mathcal{S}} \sum_{r\in\mathcal{N}_s} \beta_r (2\delta_{x_s x_r} - 1),$$

where $\delta_{x_s x_r}$ is the Kronecker δ symbol.

In this paper an MRF texture pattern is synthesized by using the Metropolis exchange algorithm as in [2, 5]. This algorithm randomly selects two different lattice sites and computes the change in energy that would occur if the two sites were exchanged, ΔE. The sites are then exchanged with probability $\min(1, \exp(-\Delta E/T))$. One iteration is counted when MN exchanges have been attempted. Note that this algorithm preserves the image histogram.

In the literature where MRF's were applied to texture modeling using the Metropolis exchange there was no consideration of temperature, i.e., (2) was given without T. However, in the application of MRF's to other computer vision problems, T is both included and varied according to some annealing schedule, typically

$$T = c/\log(\lfloor \frac{i}{i_{eq}} \rfloor + 1), \qquad (4)$$

where $i = 0,\ 1,\ \ldots$ is the iteration number, i_{eq} is the number of iterations done at each temperature for the pattern to equilibrate, and $\lfloor\ \rfloor$ performs truncation. The scale factor in the numerator is typically chosen in the range $c \in (0, 10]$. Though its choice is ad hoc, its behavior is understood as a rate constant that is proportional to how slow the annealing progresses. In this paper, we consider the direct effects of temperature on the texture pattern.

2.2 Aura Measures and Co-occurrences

In [6] we introduced the aura. The aura gives a precise mathematical meaning to the notion of how one set B is present in the neighborhood of some other set A. To measure how *much* of set B is present in the neighborhood of set A, we also introduced the aura measure. This definition is repeated here as it will be used for reformulating the MRF energy.

Definition 1 *The aura measure, denoted by $m(A, B)$, is defined by*

$$m(A, B) = \sum_{s\in A} |\mathcal{N}_s \cap B|.$$

When A and B are two graylevel sets S_g and $S_{g'}$, the aura measure will be denoted by $m(g, g')$.

The aura measure has an important relationship to co-occurrence statistics, a popular texture analysis tool. When the neighborhood structure $\mathcal{N}$ is a single element, the aura measure is a pairwise co-occurrence statistic. Taking aura measures over arbitrary $\mathcal{N}$ gives a generalized co-occurrence statistic over the neighborhood $\mathcal{N}$. If we define the *aura matrix* as the matrix $\mathbf{A}$ having element $\mathbf{A} = [a_{ij}]$ where $a_{ij} = m(i, j)$, the measure of graylevels i and j, then an aura matrix is a linear combination of co-occurrence matrices.

3 MRF's and Auras

Because the aura can be formulated using morphological dilation [7] and because of the relationship between aura measures and co-occurrences, we are able to relate MRF's to both dilation and co-occurrences by reformulating the MRF using aura measures. The reformulation also provides a physically motivated description for the ground states of the textures being modeled.

3.1 Linear Reformulation of Energy

In this section we show how the homogeneous nonlinear Gibbs energy function can be formulated as a linear combination of aura measures. The reformulation shown here is a straightforward generalization of the one given for the isotropic and anisotropic autobinomial MRF in [6].

Proposition 2 *Let $\{\mathcal{S}_g, g \in \Lambda\}$ be a partition of $\mathcal{S}$ where $x_s = g$ if $s \in \mathcal{S}_g$. Let the symmetric neighborhood $\mathcal{N}$ be partitioned into K isotropic subneighborhoods. Then any anisotropic nonlinear function of the form,*

$$\sum_{s \in \mathcal{S}} \sum_{r \in \mathcal{N}_s} V_r(x_s, x_r), \tag{5}$$

can be rewritten as a linear function of aura measures,

$$\sum_{k=1}^{K} \sum_{g, g' \in \Lambda} V^k(g, g') m^k(g, g'). \tag{6}$$

Proof: Using the assumption that $\mathcal{S}_g$ partitions $\mathcal{S}$, we can rewrite (5) as

$$\sum_{g \in \Lambda} \sum_{s \in \mathcal{S}_g} \sum_{r \in \mathcal{N}_s} V_r(g, x_r).$$

Let $V^k(g, x_r)$ be the value of $V_r(g, x_r)$ in subneighborhood k where the interaction $V_r(x_s, x_r)$ is assumed to be isotropic. Then we obtain

$$\sum_{g \in \Lambda} \sum_{s \in \mathcal{S}_g} \sum_{k=1}^{K} \sum_{r \in \mathcal{N}_s^k} V^k(g, x_r).$$

Now we partition $\mathcal{N}_s^k$ into its different graylevels. When $r \in S_{g'}$, we have $x_r = g'$, giving,

$$\sum_{g \in \Lambda} \sum_{s \in \mathcal{S}_g} \sum_{k=1}^{K} \sum_{g' \in \Lambda} \sum_{r \in \mathcal{N}_s^k \cap \mathcal{S}_{g'}} V^k(g, g'),$$

which after rearranging, becomes

$$\sum_{k=1}^{K} \sum_{g, g' \in \Lambda} \sum_{s \in \mathcal{S}_g} \sum_{r \in \mathcal{N}_s^k \cap \mathcal{S}_{g'}} V^k(g, g').$$

This is equivalent to

$$\sum_{k=1}^{K} \sum_{g, g' \in \Lambda} V^k(g, g') \sum_{s \in \mathcal{S}_g} |\mathcal{N}_s^k \cap \mathcal{S}_{g'}|,$$

which gives, finally,

$$\sum_{k=1}^{K} \sum_{g, g' \in \Lambda} V^k(g, g') m^k(g, g').$$

■

3.2 Special Cases

As before, we consider the autobinomial and Potts models. Using Proposition 2, the anisotropic autobinomial function to be maximized is

$$\sum_{k=1}^{K} \beta_k \sum_{g, g' \in \Lambda} g g' m^k(g, g').$$

The anisotropic function is simply a linear sum of isotropic functions, with weights equal to the bonding parameters. Similarly, the anisotropic Potts model gives the function

$$\sum_{k=1}^{K} \beta_k \sum_{g, g' \in \Lambda} (2\delta_{gg'} - 1) m^k(g, g').$$

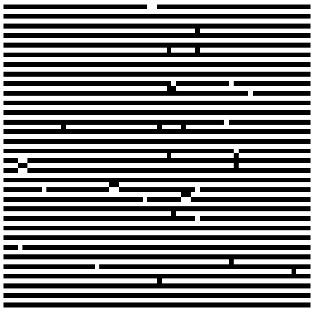

$$\mathbf{A}^1 = \begin{bmatrix} 4030 & 66 \\ 66 & 4030 \end{bmatrix}$$

$$\mathbf{A}^2 = \begin{bmatrix} 64 & 4032 \\ 4032 & 64 \end{bmatrix}$$

$$\mathbf{A} = \begin{bmatrix} 4094 & 4098 \\ 4098 & 4094 \end{bmatrix}$$

Figure 1: This 64×64 striped pattern was synthesized using a first order binary MRF with $\beta_1 = 1$ (horizontal) and $\beta_2 = -1$ (vertical). $\mathbf{A}^1$ and $\mathbf{A}^2$ are the aura matrices for the horizontal and vertical subneighborhoods, respectively. These add to give the anisotropic aura matrix, $\mathbf{A}$.

3.3 Physical Texture Behavior

With the new linear formulation, optimizing the Gibbs energy corresponds to maximizing or minimizing the individual aura measures depending on the signs of their β_k's. For low order MRF neighborhoods this corresponds to the physical notion of maximizing or minimizing boundary lengths between the gray levels.

In Figure 1 is shown an example of simultaneous boundary minimization in the horizontal direction and boundary maximization in the vertical direction. Here, the magnitudes of the bonding parameters are equal, $|\beta_k| = 1$, but the signs vary. The ground state for this anisotropic pattern will be horizontal stripes. The aura matrices for the horizontal and vertical directions are also shown. Because of the linearity of the energy, these two matrices add to give the anisotropic aura matrix.

An analogy can also be made between the behavior of the graylevel sets and the physical behavior of fluids. As the boundary between two sets is minimized they separate, i.e, each one clumps up. As the boundary is maximized, the two sets mix. This "miscibility" behavior can also be easily seen in Figure 5 (b) where the eight graylevels start out mixed, but are separated by a fourth order MRF with positive isotropic β_k.

4 Temperature and Texture

In the annealing schedule (4), the constant c determines how slow the annealing progresses. In this section, using the linear formulation, we show that the bonding parameters of the MRF act as rate constants for the annealing in each of the miscibility directions. Thus, an MRF texture pattern can be characterized by how far the mixing has proceeded in each direction.

4.1 Parameters as Annealing Rates

In the rest of this paper we just consider the autobinomial model, though a similar procedure can be followed for the Potts energy and for any other forms of $V^k(g, g')$.

Let $\mathbf{A}^k$ be the matrix of aura measures on the subneighborhood $\mathcal{N}^k$, and let $\mathbf{g} = (0, 1, \ldots, n-1)^T$. The formulation follows directly from substituting the autobinomial energy function and the iteration-dependent temperature of (4) into (2).

$$P(\mathbf{x}) = \frac{1}{Z} \prod_{k=1}^{K} \exp\left(\frac{\log(\lfloor \frac{i}{i_{eq}} \rfloor + 1)}{c} \beta_k \mathbf{g}^T \mathbf{A}^k \mathbf{g} \right).$$

Now let $T_k = \frac{c/\beta_k}{\log(\lfloor \frac{i}{i_{eq}} \rfloor + 1)}$, and $E^k(\mathbf{x}) = -\mathbf{g}^T \mathbf{A}^k \mathbf{g}$, the portion of energy in the kth isotropic subneighborhood. The anisotropic MRF can then be written as

$$P(\mathbf{x}) = \frac{1}{Z} \prod_{k=1}^{K} \exp\left(-\frac{1}{T_k} E^k(\mathbf{x}) \right). \tag{7}$$

Note that the anisotropic bonding parameters, β_k, have been absorbed into the rate constant of T_k. Effectively, each direction acts like an isotropic field: each has its own annealing rate constant, which controls its progress toward its ground state.

When the MRF is isotropic, all the rates are the same and the pattern converges equally fast in all directions. When the rates have the same magnitude but opposite signs, as in Figure 1, mixing and separation proceed at the same rate in different directions. When the rates differ in magnitude the interaction due to the anisotropic rates of mixing and separation causes interesting textures to form.

4.2 Transition Temperature

In a physical system, the environmental parameters are varied to find places where the system of interacting particles may undergo a major change in behavior such as a phase transition from liquid to solid. The point at which the transition occurs is the *critical point*; the temperature at this point is the *critical temperature*. Strictly speaking, one dimension of the lattice needs to go to infinity for a phase transition to exist. Nevertheless, the finite texture patterns still undergo behavior that is close to a phase transition.

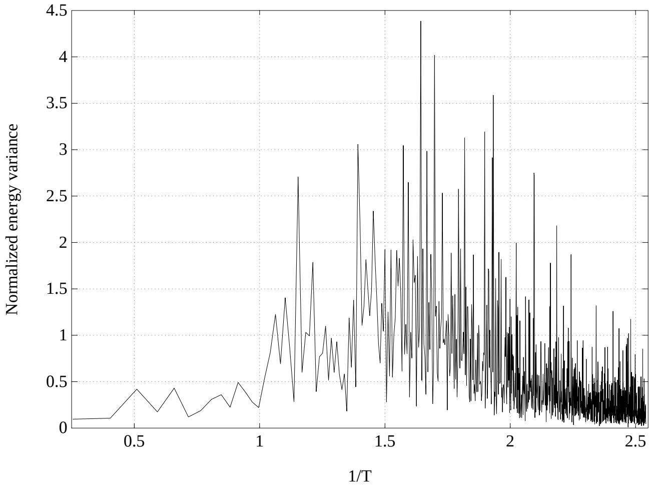

Figure 2: Plot of normalized energy variance, $C(T)$, for the binary isotropic autobinomial MRF with $\beta = 1$. The plot is made over 10000 iterations with T decreased every i_{eq}=10 iterations.

We call the temperature where the behavior changes a *transition temperature* and denote it by T_*.

Using Proposition 2 the problem of finding the transition temperature for a given set of MRF parameters can be decoupled into the problem of finding T_* for each isotropic field. We now show one method for locating T_*.

Normalizing the specific heat formula of [8] we define the normalized variance of the energy of the MRF,

$$C(T) = (< E(T)^2 > - < E(T) >^2)/T^2|\mathcal{S}|. \quad (8)$$

Since our synthesis algorithm samples with the Boltzmann factor, $\exp(-E/T)$, the evaluation of the mean of the energy at T, $< E(T) >$, is just the sum

$$< E(T) >= \sum_{i=1}^{i_{eq}} E_i(T)/i_{eq}, \quad (9)$$

where $E_i(T)$ is the Gibbs energy at the current temperature and iteration.

A typical plot of $C(T)$ is shown in Figure 2. The data in this example is from a first order binary isotropic autobinomial MRF. The samples in this plot were taken from 10000 iterations with log annealing, $c/\beta = 2.71828$ and $i_{eq} = 10$ iterations. Similar plots were obtained for $i_{eq} = 20$ and $i_{eq} = 100$ iterations with a higher average variance at the peak, but with a similar peak position.

Some texture examples for the values in this plot are shown in Figure 3, where each sample corresponds to i = 10, 100, 1000, 10000, iterations and where $1/T = 0$, 0.85, 1.7, 2.5, respectively. A quick glance reveals that

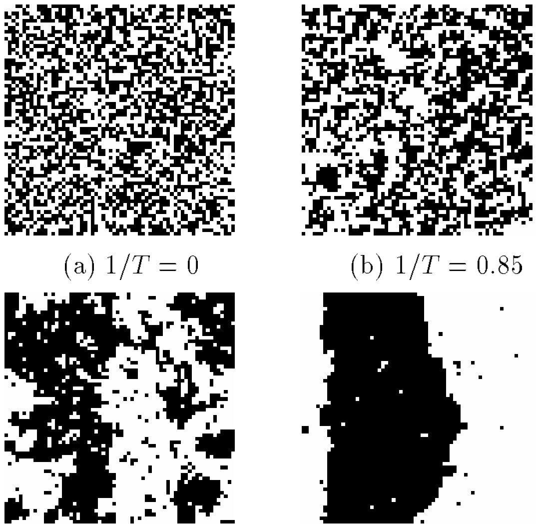

(a) $1/T = 0$ (b) $1/T = 0.85$

(c) $1/T = 1.7$ (d) $1/T = 2.5$

Figure 3: Samples of binary first-order autobinomial MRF's with isotropic bonding parameter $\beta = 1$. Images (a)-(d) correspond to 10,100,1000,10000 iterations respectively. Each image is 64×64.

to the left of the hump, the pattern does not develop much, whereas to the right, a definite separation of black and white has occurred.

One must be careful in generalizing this plot. For example, it is not accurate to conclude that synthesizing a pattern at $1/T = 1.7$ will give a texture that looks like that in Figure 3 (c). In Figure 4 is shown an example of synthesizing a sample using exactly the same parameters as in Figure 3 (c), but $1/T$ is held constant at 1.7 for 10000 iterations. Figure 4 shows that one set of MRF parameters at a single temperature can give visually different patterns. Thus, specifying the traditional MRF parameters and the temperature is not sufficient for specifying a texture pattern– it is necessary to also know how long the process has been under these conditions.

The new interpretation of parameters as annealing *rates* accounts for this evolutionary patterning. The effective rate of $1/T = 1.7$ is just to the right of the transition temperature; iterating at this temperature produces patterns which visually progress toward the ground state of total separation as in Figure 2. When the rate is further left of the hump the samples are visually similar over 100,000 iterations. Experimental simulation for $n = 2$ supports this. For $n > 2$ we have observed a corresponding increase in the number of transition peaks, as well as abrupt changes in behavior of the aura matrix structure at these peaks. This

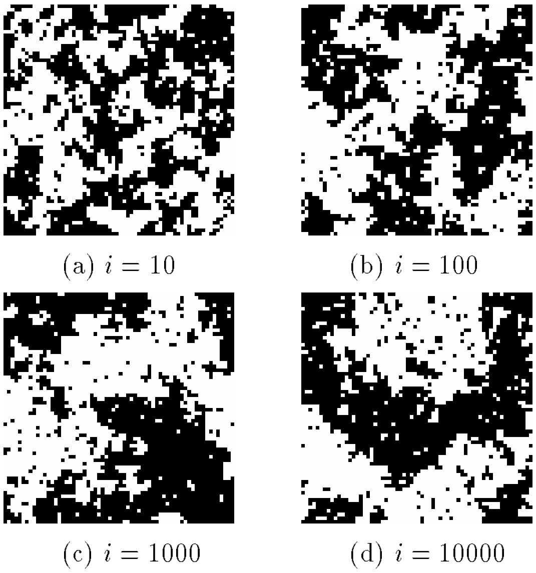

Figure 4: Samples of binary first-order autobinomial MRF's with isotropic bonding parameter $\beta = 1$. Images (a)-(d) correspond to 10,100,1000,10000 iterations respectively. All are at $1/T = 1.7$ (no annealing).

analysis is still in progress.

4.3 Texture Convergence Criteria

The number of iterations required for the texture pattern to "converge" has been a point of confusion in the literature. The confusion seems to be partly due to different definitions of convergence and equilibrium, and partly due to a lack of understanding of the effect of temperature.

For texture synthesis it is intuitively satisfying to stop the Monte Carlo iterations when the pattern has stopped changing. There are two events which will cause this: First, if it gets "stuck" in a local minimum of the energy function. Second, if it reaches its $T = 0$ equilibrium state, or "ground state". Note that when annealing is done, the texture is iterated i_{eq} times at the current temperature until it approximates a sample of the Gibbs distribution at that temperature (thermal equilibrium). However, even when the texture is in thermal equilibrium, it will be constantly changing until it reaches its $T = 0$ equilibrium state.

The texture studies in the literature have stopped the synthesis process after ten to twenty iterations stating "convergence" has occurred. In those studies [2], convergence was defined as either of the two following criteria being met: 1. The accepted number of exchanges in the Metropolis algorithm is small; 2. The estimated parameters of the sample are close to the desired parameters.

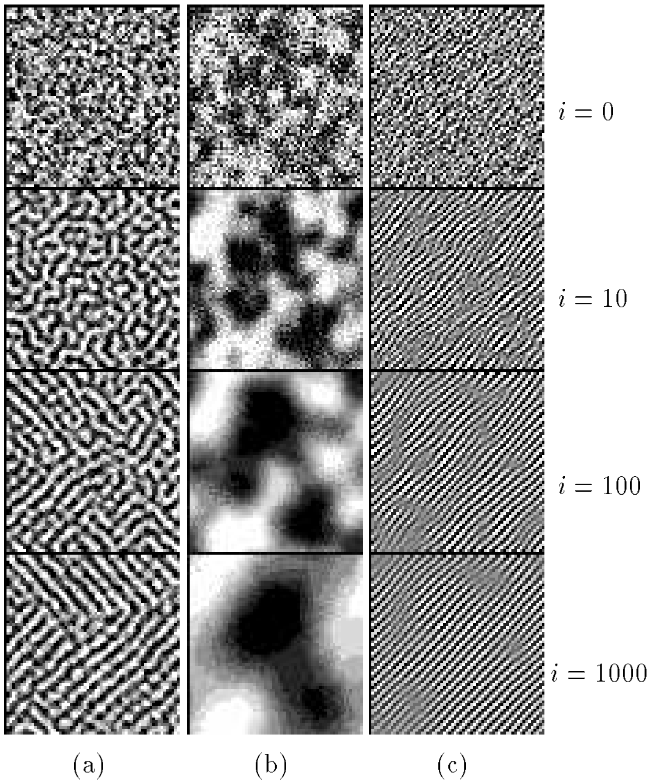

Figure 5: In each column, four 64×64 samples of an MRF are shown. All four patterns in a given column were synthesized using the same parameters. The image in the top row was printed after the 0th iteration, and the rows below it after the 10th, 100th, and 1000th iterations respectively.

The first criteria suffers from two problems: First, textures that are above the transition temperature will always have a high number of pixels swapping, even though they look visually similar. Second, if a texture gets "stuck" in a local minimum, the number of pixels swapping will satisfy the first criteria even though the MRF has not "converged" to its maximum probability configuration. The second criteria suffers from the problem that the parameters are really rates, and so do not uniquely correspond to a given texture sample.

4.4 Non-Minimum Energy Textures

As can be inferred from the convergence discussion in the preceding section, the autobinomial texture patterns studied in the literature had not converged to their minimum energy configurations. To emphasize this and reinforce the interpretation of the parameters as rates, we describe three example patterns which are not in their minimum energy states.

In Figure 5, twelve 64×64 samples with $n = 8$ are shown. Within a column, all the samples have the same set of parameters. Each was also synthesized at a constant $T = 1$. The rows correspond to sampling after the 0, 10, 100, and 1000 iterations of the Metropolis exchange algorithm. The textures in the second row were said to have "converged" according to the criteria of Section 4.3. In actuality, they are probably in equilibrium, but their patterns have clearly not stopped changing.

In column (a) of Figure 5, first and second order positive parameters cause the lines to thicken – the graylevels try to minimize their boundary, and third and fourth order negative parameters cause the lines to bend and twist – trying to maximize graylevel boundary. The relative magnitudes of the β_k control which boundary influence is more prevalent.

5 Ground State Patterns

Using the aura matrix formulation of the MRF energy, we have been able to characterize under certain conditions, the patterns which occur in the $T = 0$ equilibrium states of the isotropic autobinomial MRF. Under suitable technical assumptions the aura matrix will become tridiagonal in the positive bonding parameter case and anti-tridiagonal in the negative case [9]. The structure that appears in the aura matrix will also appear in the co-occurrence matrix; we believe that these are some of the first results relating MRF's to structure in co-occurrence matrices.

More significantly, the structure in the optimal aura matrices severely limits the textures that can be represented by the ground states of the isotropic autobinomial MRF, and to some extent, the anisotropic MRF. When the conditions are such that the matrices become tridiagonal or anti-tridiagonal, then for $n \geq 5$, the elements of the aura matrix $m(i, j)$ and $m(i, n-1-j)$ will be zero for $|i - j| > 1$. This means that graylevels j and $n - 1 - j$ cannot be neighbors of graylevel i.

If, however, the textures are sampled at non-minimum energy, all patterns are still possible. These results suggest that deterministic mean-field style algorithms which aim to provide only the ground state samples should be used with caution for texture modeling. Instead, it seems important to study the non-minimum energy states, and perhaps, focus instead on the constraints that can be used to maintain the desired pattern. There is evidence that nature forms patterns in this way – constraining physically the materials so that their minimum energy configuration is patterned [10].

6 Conclusions

We have used the new neighborhood-dependent notion of an aura measure to linearize the Gibbs energy. The aura measures allow the texture to be characterized using the physical analogy of mixing and separation. Using the linear energy reformulation we have shown that the MRF bonding parameters act as annealing rate constants in each direction of the anisotropic field. We have also given evidence for a transition temperature, below which the miscibility behavior appears to progress toward its ground state, and above which the pattern does not change much. The recognition of the transition temperature and the bonding parameter rate behavior accounts for some of the confusion in the texture literature regarding the convergence of these models.

The ground states for the autobinomial MRF can be characterized by finding the structure in the aura matrices as the texture sample converges. Finally, we pointed out that the structure in the optimal autobinomial aura matrices limits the types of textures that can be represented by the ground states of these MRFs. These limitations on the minimum energy configuration should be considered when optimizing an objective function incorporating an MRF texture model.

Acknowledgments

R. W. Picard would like to thank Roland R. Netz for interesting and helpful discussions on Gibbs energy equilibrium. I. M. Elfadel wishes to acknowledge the support and encouragement of Prof. John Wyatt, Jr.

References

[1] J. Besag. Spatial interaction and the statistical analysis of lattice systems (with discussion). *J. Roy. Stat. Soc., Ser. B*, 36:192–236, 1974.

[2] G. R. Cross and A. K. Jain. Markov random field texture models. *IEEE T. Patt. Analy. and Mach. Intell.*, PAMI-5(1):25–39, 1983.

[3] S. Geman and D. Geman. Stochastic relaxation, Gibbs distributions, and the Bayesian restoration of images. *IEEE T. Patt. Analy. and Mach. Intell.*, PAMI-6(6):721–741, 1984.

[4] H. Derin and H. Elliott. Modeling and segmentation of noisy and textured images using Gibbs random fields. *IEEE T. Patt. Analy. and Mach. Intell.*, PAMI-9(1):39–55, 1987.

[5] L. Garand and J. A. Weinman. A structural-stochastic model for the analysis and synthesis of cloud images. *J. of Climate and Appl. Meteorology*, 25:1052–1068, 1986.

[6] I. M. Elfadel and R. W. Picard. Miscibility matrices explain the behavior of grayscale textures generated by Gibbs random fields. In *Proc. SPIE Conf. on Intell. Robots and Comp. Vis.*, volume 1381, pages 524–535, Boston, MA, Nov. 1990.

[7] I. M. Elfadel and R. W. Picard. Auras part I: Theory and relation to morphology and co-occurrence. Technical report, MIT Media Lab, Vision and Modeling TR #149, Feb. 1991.

[8] S. Kirkpatrick, C. D. Gelatt, Jr., and M. P. Vecchi. Optimization by simulated annealing. *Science*, 220(4598):671–680, 1983.

[9] R. W. Picard. and I. M. Elfadel On the structure of optimal aura matrices. Technical report, MIT Media Lab, Vision and Modeling TR #160, Feb. 1991.

[10] T. Tanaka, S-T. Sun, Y. Hirokawa, S. Katayama, J. Kucera, Y. Hirose, and T. Amiya. Mechanical instability of gels at the phase transition. *Nature*, 325(6107):796–798, 1987.